Chiral Discotic Columnar Germs of Nucleosome Core Particles

Françoise Livolant and Amélie Leforestier
Laboratoire de Physique des Solides, Université Paris Sud, 91405 Orsay Cedex, France

ABSTRACT In concentrated solution and in the presence of high concentrations of monovalent cations, nucleosome core particles order into a discotic columnar mesophase. This phase is limited to finite-sized hexagonal germs that further divide into six coiled branches, following an iterative process. We show how the structure of the germs comes from the competition between hexagonal packing and chirality with a combination of dendritic facetting and double-twist configurations. Geometrical considerations lead us to suspect that the chirality of the eukaryotic chromosomes may originate from the same competition.

INTRODUCTION

In eukaryotic chromatin, proteins associate with DNA and condense the molecule into the nucleosomic filament made of the succession of nucleosome core particles linked together by DNA segments. This filament is itself compacted into higher order structures through the association with other proteins, namely H1 histones. The supramolecular organization of this filament is still not completely understood, but the structure of the nucleosome core particles (NCPs) is well established. It is composed of an octameric protein core containing two copies of each histone (H2A, H2B, H3, and H4), around which 146 bp of DNA coils over 1.75 turn in a left-handed superhelix. The global shape of the particle, the crystallographic structure of which has been solved at 2.8-Å resolution (Luger et al., 1997), is that of a flattened cylinder 10.5 nm in diameter and 5.7 nm in height. The DNA-histone association is essentially due to electrostatic contacts between the DNA phosphate negative charges and the basic (Lys + Arg) residues of the histones. The complex is itself highly negatively charged. We showed recently that these particles may form in vitro multiple liquid crystalline phases, depending on the particle concentration and on their ionic environment (Leforestier and Livolant, manuscript in preparation). In the presence of high amounts of monovalent salts, NCPs organize spontaneously into a columnar hexagonal discotic mesophase (Leforestier and Livolant, 1997). Owing to the chiral nature of the particles, a competition is expected to occur between the hexagonal dense packing of the columns and the tendency of molecules to twist. In this article, we show how this competition leads to the formation of helical germs with a sixfold symmetry. These experimental results are compared to theoretical predictions (Kléman, 1985; Yan and Lubensky, 1997; Kamien and Nelson, 1995, 1996). Coming back to biology, we hypothesize that a similar competition process is involved in vivo and could be responsible for the helical nature of the mitotic chromosomes.

Received for publication 1 November 1999 and in final form 17 February 2000.

Address reprint requests to Dr. Françoise Livolant, Laboratoire de Physique des Solides, Bât 510, Université Paris Sud, 91405 Orsay Cedex, France. Tel.: 33-1-69-15-53-92; Fax: 33-1-69-15-60-86; E-mail: livolant@lps.u-psud.fr.

0006-3495/00/05/2716/14 $2.00

MATERIALS AND METHODS

Preparation of nucleosome core particles

Large amounts of NCPs were prepared from native calf thymus chromatin. H1-depleted chromatin was selectively digested with micrococcal nuclease (Pharmacia), and the NCP fraction was purified by gel chromatography over Sephacryl S 300 (Pharmacia). The histone composition was checked by sodium dodecyl sulfate gel electrophoresis on 15% (w/v) acrylamide gels. The purity of the NCP fraction as well as the integrity of the particles were checked by retardation electrophoresis on 7.5% acrylamide gels. The samples were shown to be devoid of contaminant proteins, di- and oligonucleosomes, and free DNA fragments (not shown). The DNA was extracted from the purified fraction. It migrates in polyacrylamide gel as a 146-bp single band, indicating that the length variation of the nucleosomal DNA does not exceed a few base pairs.

NCPs were suspended in buffer solutions (10 mM Tris-HCl, 1 mM EDTA, added with 100 or 150 mM NaCl). The solutions were concentrated up to 275 mg NCP/ml by ultrafiltration under nitrogen pressure (2 bars) throughout a porous membrane (Amicon; YM 100 in a 8010 pressurized cell).

Higher concentrations were reached in one of two ways:

1. Under controlled osmotic pressure, by direct mixing with a neutral incompatible polymer (PEG 8000 dissolved in the same buffer). This method yields equilibrium samples in which the NCP liquid crystal phase separates from the surrounding polyethylene glycol. By this method, the ionic concentration is controlled and kept constant (100 or 150 mM).

2. By slow dehydration of the solution. The method yields nonequilibrium samples where the NCP liquid crystalline germs are observed to be growing in the isotropic phase. In this case, the increase in the NCP concentration is accompanied by a proportional increase in salt concentration. This varies from 100 or 150 mM to ~300 mM, as was estimated from the value of the NCP concentration (calculated from the lattice parameters of the ordered phase).

Similar results were obtained by the two preparation procedures. The illustrations presented here were recorded on specimens prepared by procedure 2.

Polarizing microscopy

Drops of the solutions were deposited between slide and coverslip and sealed either immediately or later on, depending on the requirements. Preparations were allowed to stabilize for days to months at room temperature. Observations were made on a Nikon Optiphot X Pol microscope between crossed linear or circular polars. A lambda plate (λ) was used to

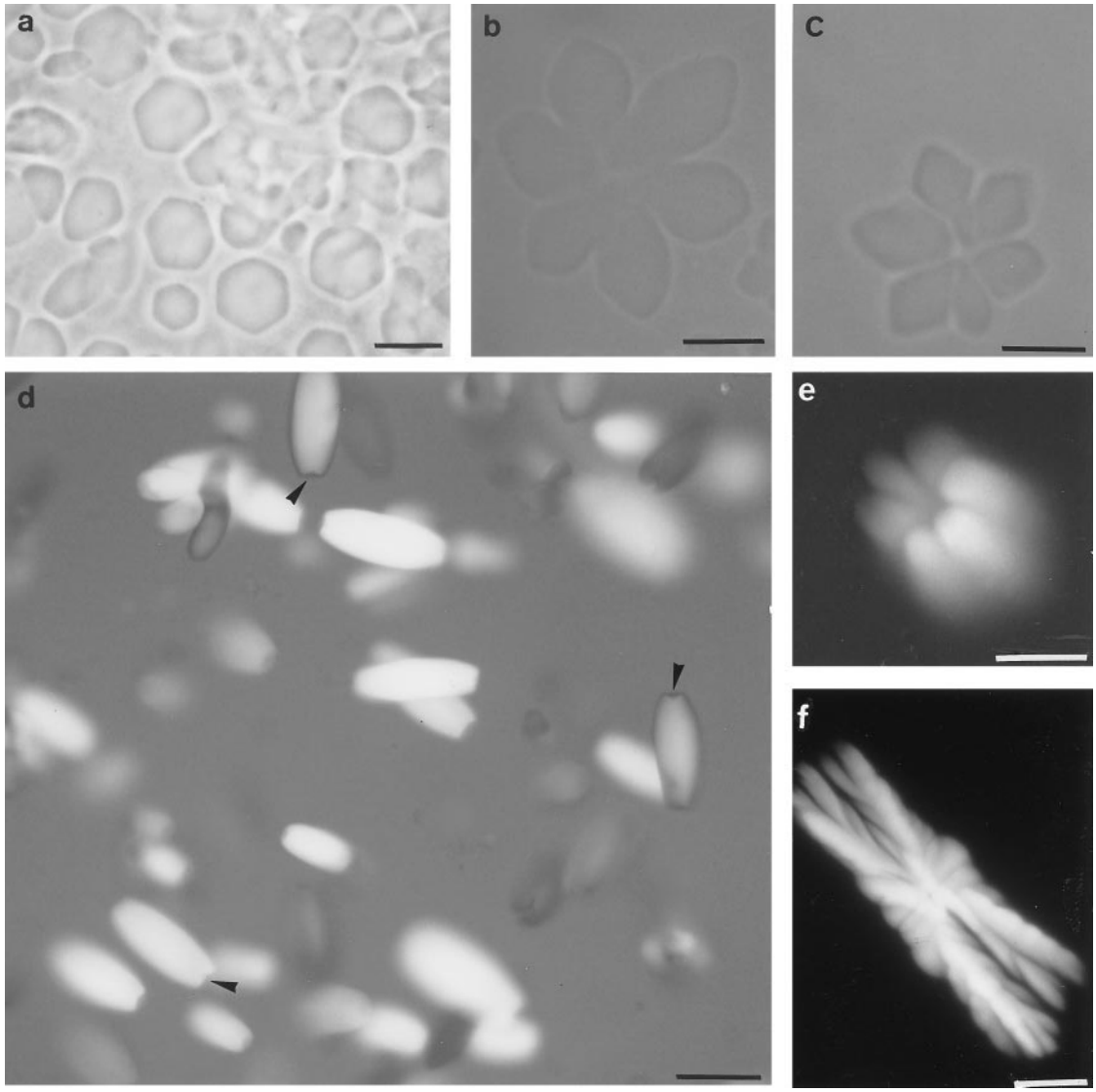

FIGURE 1 Nucleation and growth of the hexagonal germs of NCP observed in optical microscopy. (*a–c*) Apical views of the hexagonal germs growing in the isotropic solution. (*a*) Small germs with a perfect hexagonal shape (phase-contrast microscopy). (*b*) Larger germs keep their sixfold symmetry shape but transform into flower-shaped patterns (parallel polars). (*c*) Germ in which the six parts appear disconnected (parallel polars). (*d*) Lateral views of the germs growing freely between slide and coverslip. Note the depressions at both of their extremities (*arrowheads*). The homogeneous colors of the germs (either blue or yellow, depending on their orientation relative to λ) reveal the unidirectional orientation of the columns (crossed polars, λ). (*e*) Oblique view of a germ showing its six individualized branches (crossed polars). (*f*) Side view of an elongated germ growing in a very thin preparation that prevents its three-dimensional growth. While extending, the extremities of the germ diverge and show dendrite shapes (crossed polars). Scale bars: *a* and *f*: 20 μm; *b–e*: 10 μm.

determine the orientation of DNA and consequently of the columns of nucleosome cores inside the germs.

Freeze-fracture electron microscopy

Samples were deposited on gold supports, allowed to stabilize under a humid atmosphere for 30–90 min, and quenched at 10 K by projection onto a copper block with a cryovacublock device (Reichert). Freeze fracture was performed under a 2×10^{-7} Torr vacuum in a Balzers BAF 400T apparatus. After 2 min of etching at 153 K, the surface was shadowed with Pt evaporated at an angle of 45° and carbon coated. After heating to room temperature, replicas were washed in distilled water and observed in a Philips 400T transmission electron microscope at an accelerating voltage of 80 kV. Owing to the short stabilization time of the samples before freezing, the diameter of the germs observed in electron microscopy was systematically lower than 1 μm, while it can reach up to 50 μm after days to months of stabilization (optical microscopy experiments).

RESULTS

Structure of the columnar hexagonal germs

Multiple germs were observed to be nucleating and growing within the isotropic solution. The smaller ones usually present either of the following shapes:

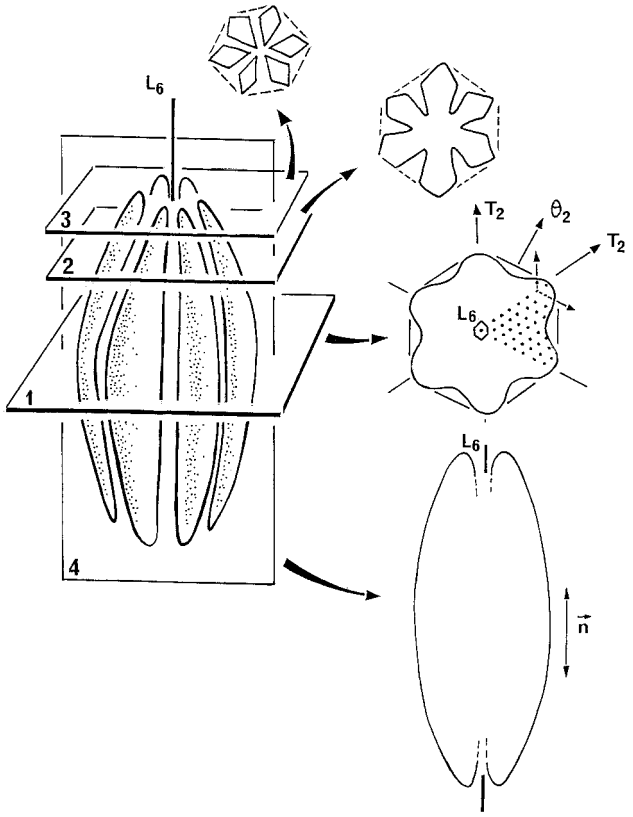

FIGURE 2 Schematic representation of the structure of the small germs. The rodlike germs are made of six individualized branches connected together in the median plane. They appear elongated when the observation plane is parallel to their elongation axis (*plane 4*). Their hexagonal shape can be seen when the observation plane is normal to the elongation axis of the germ (*planes 1, 2*, and *3*). The six strands may or may not appear to be connected. Symmetries of the columnar hexagonal structure are shown: twofold symmetry axes T2 and $\theta 2$, and sixfold symmetry axis L6. Growth occurs preferentially along the T2 directions of the hexagonal network.

1. A regular hexagonal shape easily observed in phase-contrast microscopy (Fig. 1 *a*). They are nearly extinguished between crossed polars but can be turned illuminated by gently moving the slide with respect to the coverslip. The germs thus distort and elongate along the sliding direction.

2. Elongated shapes (Fig. 1 *d*) with a small depression at their extremities. These germs are highly birefringent and turn blue when a first-order retardation plate is inserted in the microscope and aligned parallel to the axis of the germ.

Both kinds of germs correspond to a unique structure in which NCPs are piled on top of each other to form columns, these columns being aligned in parallel in a 2D hexagonal network, leading to a columnar hexagonal liquid crystalline structure (Leforestier and Livolant, 1997).

A 3D reconstruction, elaborated from the observation of a large number of germs, is given in Fig. 2. They are elongated rods, with their sixfold symmetry axis (*L6*) oriented parallel to their elongation axis. The NCP columns are parallel to the *L6* axis, leading, between crossed polars, to the extinction of the germs in a top view (DNA coiled around the NCP particles showing all possible orientations in the preparation plane) and their illumination in a side view (DNA being, on average, normal to the elongation axis). In the top view, hexagonal patterns are seen with different aspects, depending on the focus plane: 1) hexagons in the median plane (*plane 1*), 2) crenulated hexagons (*plane 2*), or 3) six isolated domains (*plane 3*) out of this plane. When observed in side view, they show an elongated shape (*plane 4*). Each of the micrographs in Fig. 1 can be attributed to one of these observation planes: Fig. 1 *a*, plane 1; Fig. 1 *b*, plane 2; Fig. 1 *c,* plane 3; Fig. 1 *d*, plane 4. Oblique views are also found in the preparation (Fig. 1 *e*) and corroborate these observations.

In thin preparations (5–10 μm), the growth of the germs usually occurs in two dimensions. Their shape then depends on the initial orientation of the columns (*n*) with respect to the observation plane, as schematically drawn in Fig. 3. When columns align normal to the preparation plane (Fig. 3 *a*), the growth is faster along the T2 directions of the lattice, thus leading to characteristic flower-shaped patterns (Fig. 1 *b*). This growth is typical of hexagonal discotic germs and

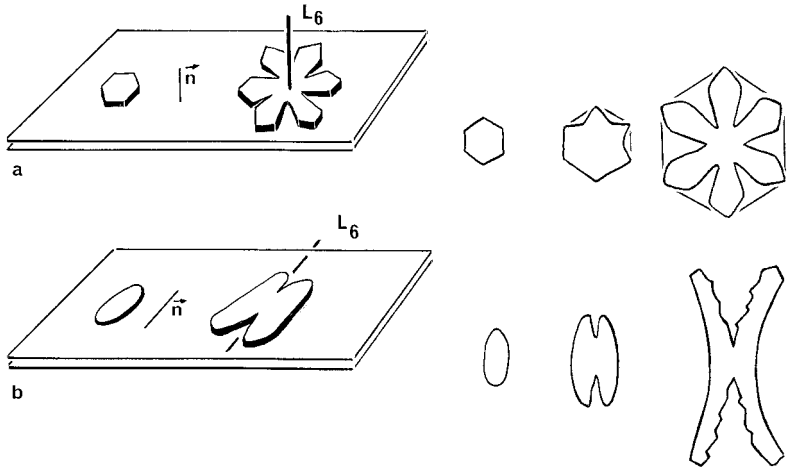

FIGURE 3 When confined between slide and coverslip, the germs grow in two dimensions. They form hexagonal platelets when the direction of the columns (*n*) axis lies normal to the preparation plane (*a*) and elongated rods with possible dendritic shapes when the columns are oriented parallel to the preparation plane (*b*). Each column is formed by the piling of NCP on top of each other.

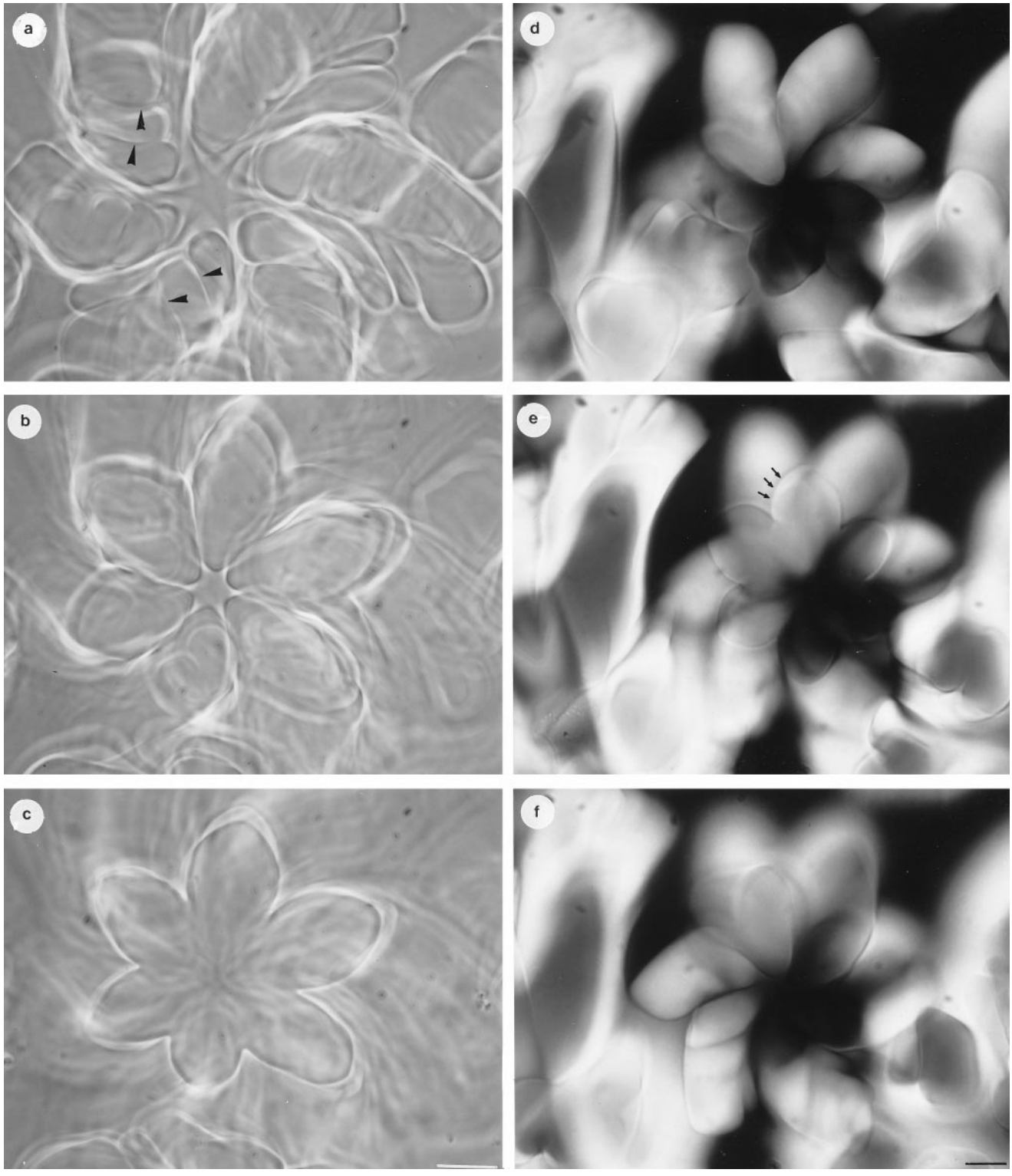

FIGURE 4 Focal series of two large germs in apical view, in phase-contrast microscopy (*a–c*) and in polarizing microscopy (*d–f*). (*a–c*) The classical flower shape of the germ seen in *c* transforms into complex patterns as the micrographs are taken higher in the preparation. First, six branches individualize and an empty core appears in between (*b*). Then, each branch presents a curved shape and appears to be made of different domains, separated by twist walls (*a, arrowheads*). Phase-contrast microscopy. Scale bar, 20 μm. (*d–f*) In the median plane (*e*) the limit of the germ (*arrow*) forms a flower shape. Below (*f*) and above (*d*), branches individualize and show curved shapes of opposite orientations (crossed polars). Scale bar, 10 μm.

has already been described in detail (Bouligand, 1980a). When columns align parallel to the preparation plane (Fig. 3 *b*), their growth leads to complex dendritic patterns with a bilateral symmetry, as shown in Fig. 1 *f*.

Macroscopic chirality of the germs

Macroscopic chirality is absent in the 2D germs, as it is in most small germs (5–10 μm in diameter), whereas it is systematically observed in large 3D germs. These chiral germs, which can reach up to 50–100 μm in diameter, were obtained in thick preparation (100 μm) by extremely slow concentration of the solution (from 6 months to a full year) (Figs. 4 and 5). Focal series were recorded from a top view of more than 25 germs, and two of them are presented here in phase-contrast microscopy (Fig. 4, *a–c*) and in polarizing microscopy (Fig. 4, *d–f*). The simple hexagonal shape can be recognized in the median plane of the germ (Fig. 4, *c* and *e*). For other focus planes, six branches separate and delimitate a central hole, which is easily visible in phase-contrast microscopy (Fig. 4 *b*). In projection onto the focus plane, the branches show crescent shapes whose concavity is reversed on both sides of the median plane of the germ (Fig. 4, *d–f*). From these observations, we see that the branches are not straight but follow helical paths with a left-handed helicity (determined from the focal series). When the branches reach 10–15 μm in diameter, each branch itself divides into six parts, which also coil around each other in a left-handed helix, following an iterative process. These top-view germs are no longer extinguished between crossed polars: NCP columns, which are parallel to the optical axis of the microscope in the median part of the germ, turn oblique to this direction because of the curvature of the branches. The addition of a λ plate shows color variations from branch to branch and inside each branch (not shown). From these colors, we determined the orientation of DNA in each branch and deduced a double-twist organization of columns, inside each branch and between branches inside the full germ. Side views of the germs corroborate the top-view observations: branches present a left-handed he-

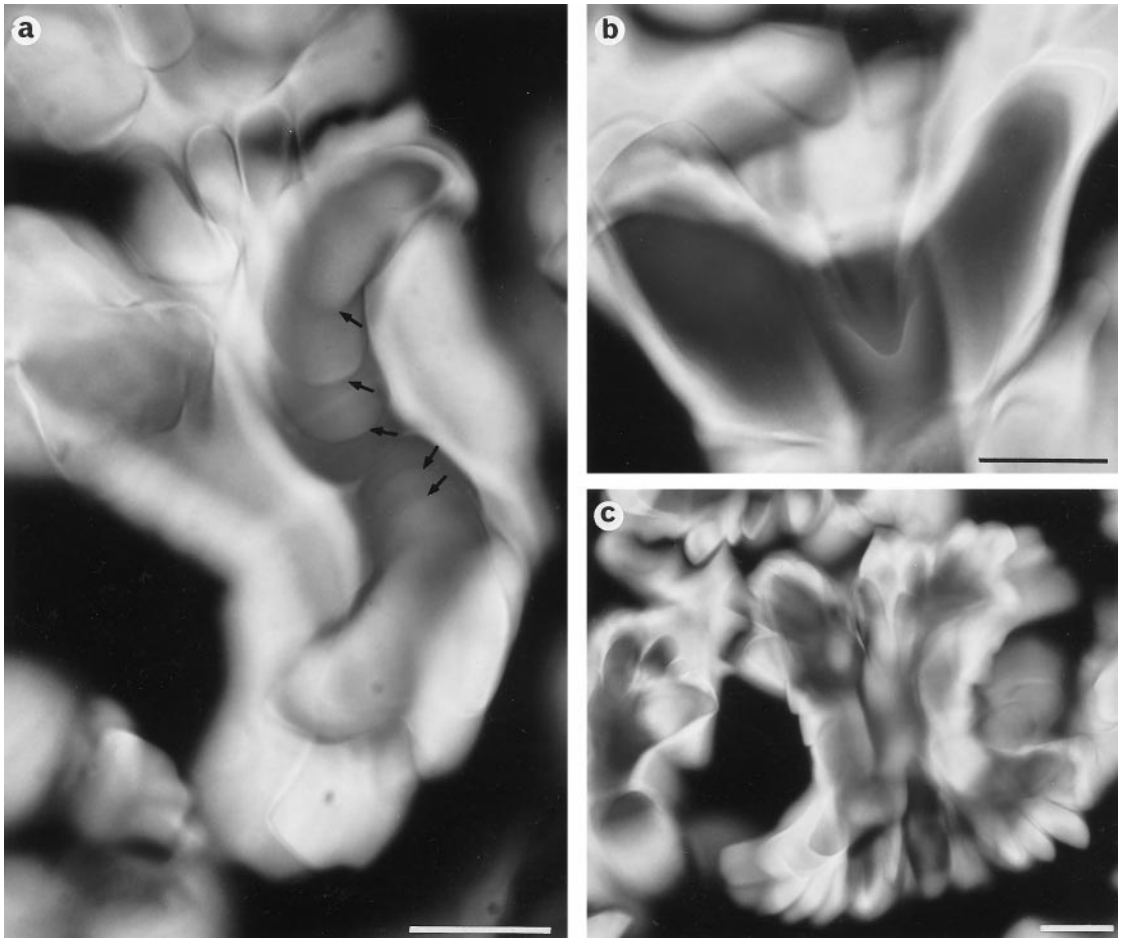

FIGURE 5 Lateral views of the large hexagonal germs. In *a*, one of the branches can be followed, with regularly arranged twist walls (*arrows*). In *b*, an enlarged view of the center of the germ shows how the branches join together. In *c*, a general view shows that the diameter of the germ is smaller in its median part than at its two extremities, where strands divide in an iterative way and diverge. Crossed polars, $\lambda/4$. Scale bars, 20 μm.

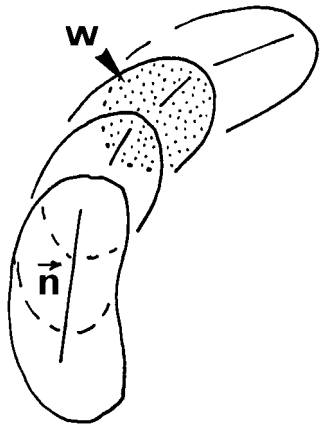

FIGURE 6 Schematic representation of domains separated by twist walls (*w, gray zone*). The orientation of the columns (*n*) rotates from one domain to the next in a right-handed way.

licity (Fig. 5 *a*). They diverge from the axis of the germ and are composed of a series of domains piled on top of each other, with the formation of twist walls (*arrows* in Figs. 5 *a* and 6). The twist is right-handed, as deduced from the analysis of focal series. The connection of the branches can be seen in the central part of the germ (Fig. 5 *b*). The overall shape of the large chiral germs is that of a diabolo (Fig. 5 *c*).

Another type of chiral germs was observed in a few preparations. They are small (maximum 6 μm wide and 15 μm long) and appear in side view, illuminated between crossed polars (Fig. 7, *a–c*). Their helical structure is revealed by oblique striations, the orientation of which depends on the focus plane (intermediate focus levels cause crossed patterns to appear (germ pointed out by the *arrow* in Fig. 7 *b*). The determination of the helical handedness is difficult because of their small size, but in two cases it was unambiguously shown to be left-handed. In one case, it was possible to count a number of six birefringent strands, thus establishing their sixfold symmetry. The diameter of each helical branch varies from 0.7 to 2 μm, with a pitch of 3.4 to 9 μm, respectively. Compared to the germs described above, they present two particularities: 1) their helical structure is clearly expressed despite their small size, and 2) the helical strands follow true helical paths, leading to a global cylindrical shape of the germ.

Ultrastructural analysis of the germs

The ultrastructure of the germs was investigated by the freeze-fracture method, which is well adapted to the study of columnar phases, which behave like lamellar structures. The planes that offer the weakest resistance to the fracture correspond to the reticular planes of the hexagonal phase (Livolant, 1991). For any oblique fracture plane, the resulting fracture surface looks like a complex staircase, with domains alternatively parallel and normal to the columns. The length (l) of the steps is defined by the angle α separating the fracture plane (F) and the column direction (n) and by the distance (d) separating the reticular planes, according to the relation $l = d/tg\alpha$ (Fig. 8). In projection onto the observation plane P, not necessarily parallel to F, periodic patterns are observed. Their periodicity x, with $x = l' + d'$ (where l' and d' are, respectively, the projections of l and d onto this plane), equals $d \cos \beta / \sin \alpha$, where β is the angle between F and the projection plane P. In a regular hexagonal phase, x remains constant when d and n are defined. Note that the lengths of l' and d' may vary with respect to each other and that the patterns may be compli-

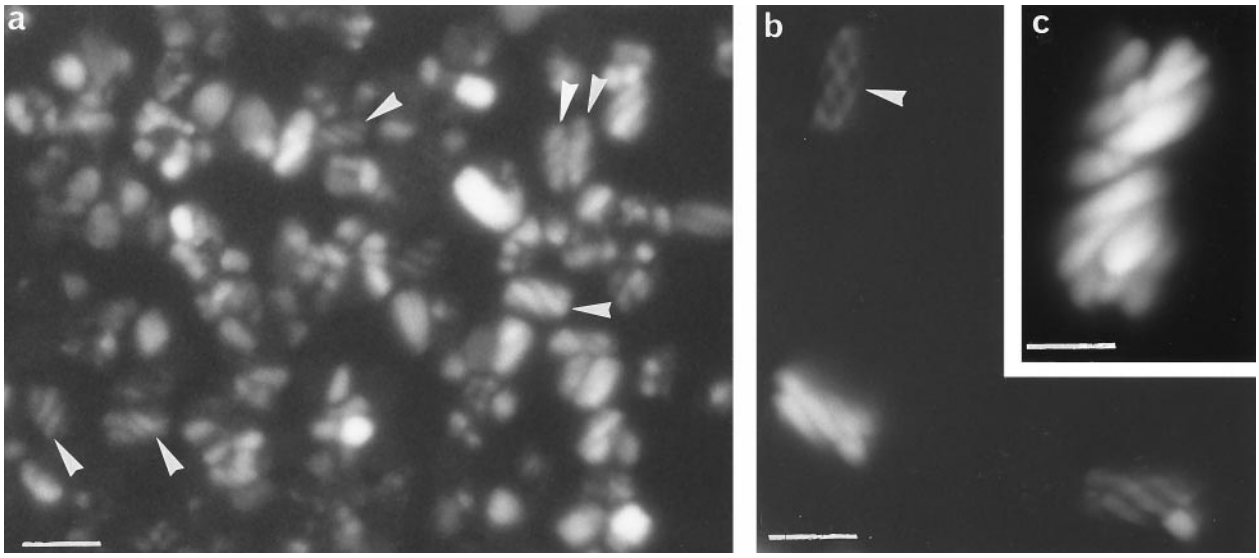

FIGURE 7 Population of small germs, a lot of them showing a helical shape (*arrowheads*), with multiple strands coiled around each other. The crossed pattern (*arrowhead* in *b*) is due to the superposition of the strands at the upper and lower levels of the germ (crossed polars). Scale bar, 10 μm.

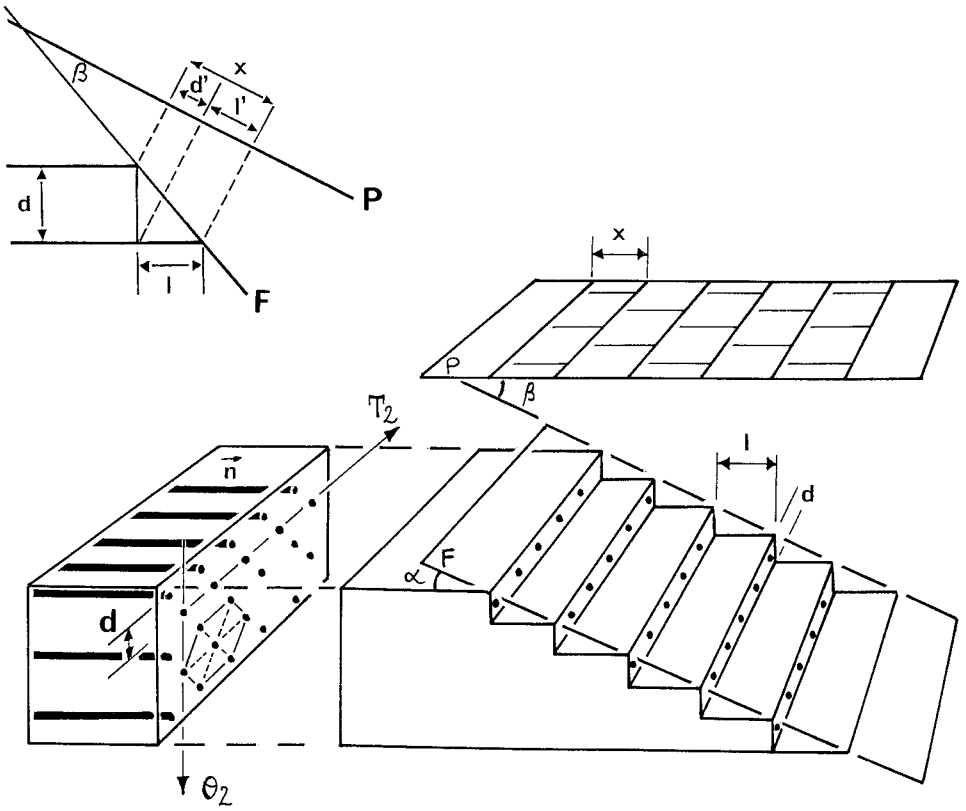

FIGURE 8 Freeze fracture of a perfect columnar hexagonal phase. For any fracture plane (F) oblique to the direction of the columns (n), the fracture progresses by steps. Their height (d) is constant and corresponds to the distance separating the reticular planes. Their length (l) depends on the obliquity of the fracture plane. In projection onto any observation plane (P), the observed periodicity x (where $x = d' + l'$, the projections of d and l) equals $d \cos \beta / \sin \alpha$, where α is the angle between n and F and β is the angle between F and P.

cated by the unidirectional shadowing effect. In our experiments, we measured x, and we supposed β to be small; therefore x is supposed to be close to $d/\sin \alpha$.

In some germs, the fracture propagates as in a perfect columnar hexagonal phase (Fig. 9, a and a'). We observe a series of parallel bands separated by steps. The steps are more or less parallel to each other, and the average width of the band (x) remains more or less constant over the whole germ. In each of these bands, the columns of nucleosomes can be seen. They follow a direction (n), which remains constant within a band and from band to band. As explained above, one band corresponds to one reticular plane of the hexagonal structure, and we follow one T2 direction when moving along a band. Passing from one band to the next means that we are moving down in the structure from one reticular plane to the next along a $\theta 2$ direction.

In many germs, deviations from this ordering are observed (Fig. 9, b and b'). The series of steps form curves instead of straight lines, and each band, delimited by two steps, enlarges progressively from one side of the germ to the other side. Taking into account that there is no significant change in the orientation of the fracture plane, the progressive increase in x reveals that the orientation of the columns changes progressively along the diameter of the germ, from close to parallel (*side A*) to close to normal (*side A′*). Therefore, twist occurs between columns along this T2 direction (~0.5° per column). When looking carefully at the orientation of the columns (n) within each band, we see that their orientation also diverges slightly, revealing a splay of ~0.5° per column. When moving from band to band along the axis of the germ (from B to B'), i.e., along a $\theta 2$ direction, the orientation of the columns also rotates progressively, leading to the formation of portions of arches. Columns in successive reticular planes therefore rotate, revealing the presence of a regular twist (~1.1° per layer). Along this direction, x also increases; the layers are close to normal in B and more oblique in B'. This means that the layers diverge slightly (~1° per layer). This is confirmed by the examination of germs such as that of Fig. 9, c and c'. The fracture plane is nearly normal to the sixfold axis and, contrary to what is expected in a regular hexagonal structure, the three main directions of the hexagonal network do not form straight lines but curves.

Deviations from perfect hexagonal ordering can easily be understood when they are considered individually as sketched in Fig. 10. How splay and twist change the periodicity of the freeze-fracture patterns is illustrated on Fig. 11, a and b. This analysis shows in the germs the occurrence of twist and splay along two directions of the hexagonal lattice (T2 and θ_2) and therefore along all directions. The measured twist values (0.5 to 1°/column in the T2 direction and 1 to 1.5°/layer in the $\theta 2$ direction) correspond to helical pitches of the order of 5 μm, taking an interhelix distance a equal to 11.55 nm and an interlayer distance

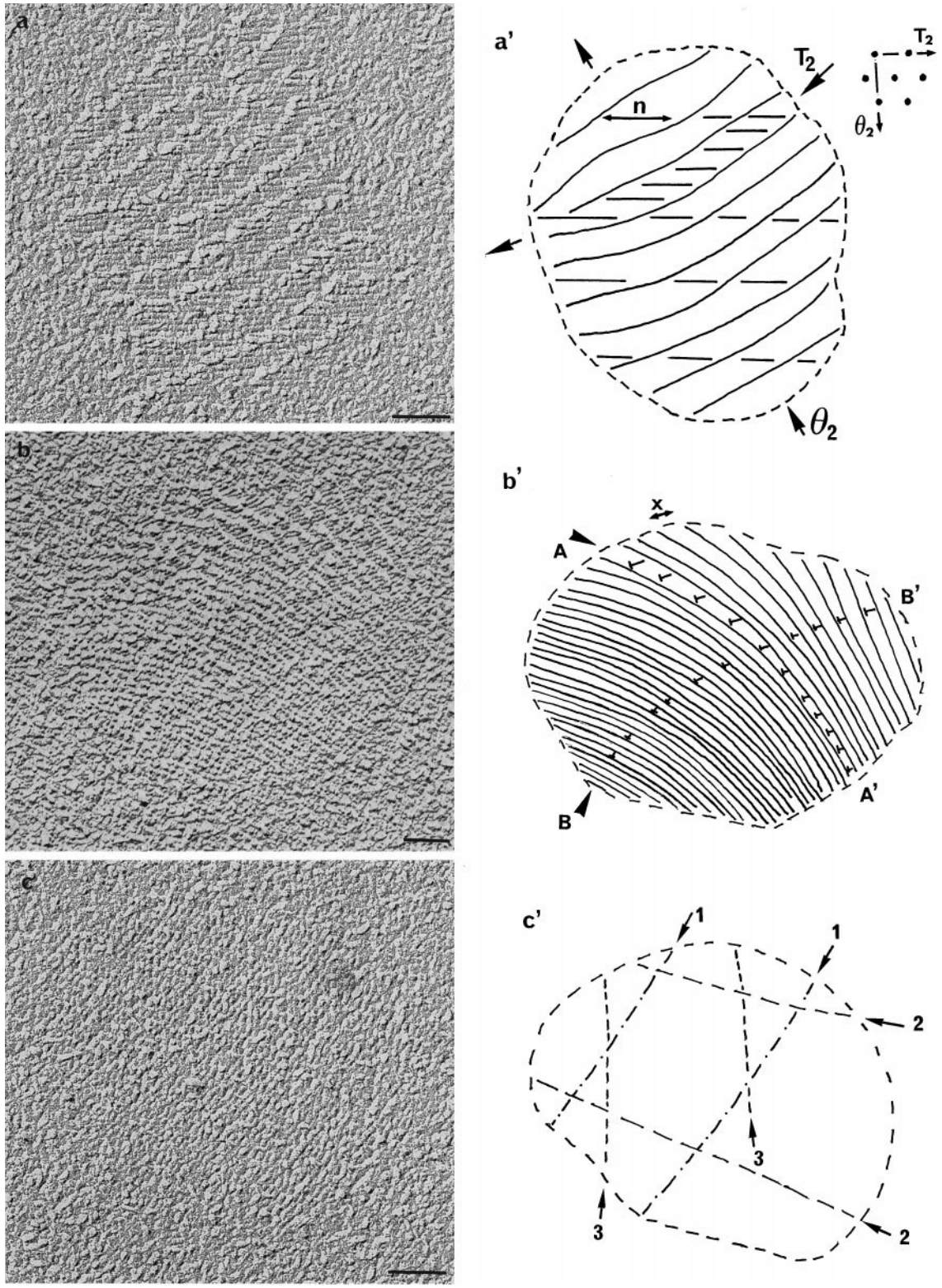

FIGURE 9 Freeze-fracture electron microscopy patterns of hexagonal germs (*a–c*) with their corresponding schematic representations (*a′–c′*). Scale bars, 100 nm. (*a, a′*) Oblique fracture plane of a "perfect" columnar phase. The steps separate different bands along which the orientation *n* of the parallel columns can be recognized. *n* remains constant from plane to plane. (*b, b′*) Oblique fracture plane of a germ showing distortions from the classical hexagonal packing. Orientations of the columns have been represented along two axes of the section of the germ (*AA′* and *BB′*), using the nail convention. (*c, c′*) Fracture plane more or less normal to the hexagonal network. The three main directions of the hexagonal network have been underlined (*1, 2, 3*). Two of them are more easily followed because of the unidirectional shadowing.

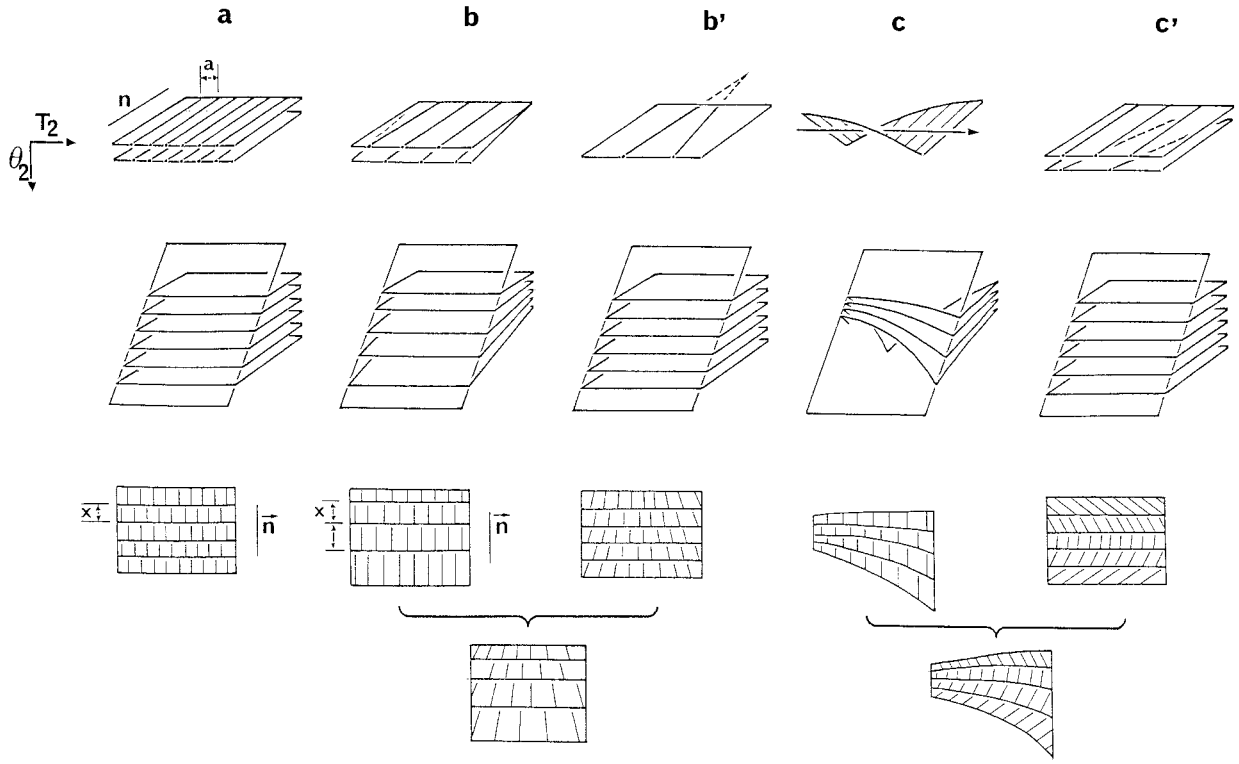

FIGURE 10 Simple cases of deviations from a perfect columnar hexagonal ordering. In *a*, a series of reticular planes, with molecules aligned along a direction *n* and separated by a distance *a*, is fractured obliquely. Parallel series of bands are observed that are of equal length (*x*), with a unidirectional orientation of the columns (*n*). When splay occurs between columns of successive layers (*b*) or between columns in a given layer (*b′*), the fracture plane crosses the successive layers at increasing distances, leading to steps of increasing length (*x*), while *n* remains unidirectional, or to steps of equal length (*x*) with different orientations of *n* on each step. If, as expected, splay is not restricted to a particular direction, complex patterns will be obtained: irregular step lengths and divergence of *n*. Consequences of twist between columns of a given reticular plane (*c*) or between successive layers (*c′*) can be seen in the same way. In *c* twist between columns leads to the deformation of the reticular plane into a helicoid. Any fracture plane parallel to the twist axis intersects the series of layers at different angles (*x* variable), while *n* remains unidirectional. Note that this situation of twist also introduces splay between the columns. In *c′* twist occurs between successive layers. Because the layers remain parallel to each other, *x* remains constant but *n* rotates from plane to plane and forms series of arches. This situation is well known in cholesteric structures.

$d = a(\sqrt{3}/\sqrt{2}) = 10$ nm (Leforestier and Livolant, 1997). From the measured splay values (~0.5°/column along the T2 and up to 1.5°/layer along the $\theta 2$ directions) we can estimate that the number of layers and columns is duplicated roughly every 0.5 μm and 2 μm, respectively. As discussed below, these values cannot directly account for the macroscopic characteristics of most germs.

DISCUSSION

The question of competition between chirality and 2D ordering in columnar phases has long been debated. A local hexagonal ordering may coexist with a long-range cholesteric organization in mesophases of helical polymers such as DNA, PBLG, or xanthan, as established experimentally by x-ray diffraction (Robinson et al., 1958; Samulski and Tobolski, 1974). Theoretically, Kléman (1985) proposed two cylindrical geometries of molecular arrangements achieving a good compromise between these two incompatible tendencies. He argued that both situations were observed experimentally in DNA systems (Livolant, 1984). Later on, Lubensky and collaborators (Yan and Lubensky, 1997; Kamien and Nelson, 1995, 1996) considered the same question again in discotic columnar systems. In some cases, the twist can simply be expelled from the columnar phase, but if the coupling between chirality and the columnar lattice is strong enough, complex phases are expected. Considering the average molecular orientation normal to the columns, they calculated that chirality could induce either a rotation of molecules inside each column, though keeping a fixed lattice structure (soliton phase), or a rotation of the columns themselves (moiré phase) when the coupling is higher. The authors also assumed additional phases to occur if the constraint that the molecular normal be parallel to the columnar axis is relaxed. In our experimental conditions, the diameter of the NCPs lie more or less normal to the columns, and the above situation does not apply. The chiral phase is limited to germs of a finite size. We never observed double twist-cylinders, the existence of which has been reported in other systems (in DNA, for example Leforestier

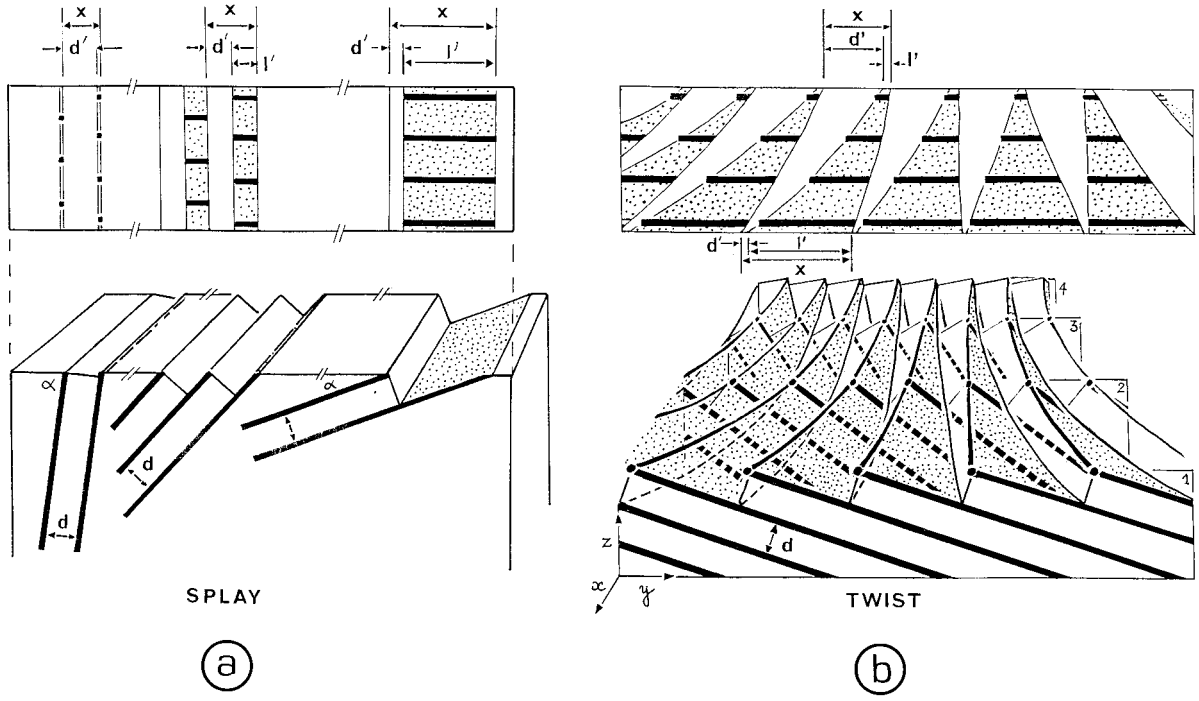

FIGURE 11 Drawing showing how changes in periodicities x of the freeze-fracture patterns may correspond either to splay (a) or to twist (b).

and Livolant, 1994). The original feature lies in the subdivision of the germs into six coiled branches.

The individualization of six branches apparently originates from the combination of two properties of the system: 1) double-twist ordering of columns, which allows a defrustration but imposes a limited lateral extension of the domains, and 2) surface tension effects, which favor the lateral extension of the germ along some reticular planes of the hexagonal lattice, leading to facetting of the germs and, further, to the formation of six domains connected together in the center. Let us follow what happens during the growth of a germ. First, the orientation of the columns rotates regularly with respect to the initial *L6* axis along any diameter in a pure double-twist configuration. While growing, the obliquity of the columns increases at the surface. Before this obliquity reaches the maximum angle (in the range of 45–65° for the general case of the double-twist cylinder, as explained by Wright and Mermin, 1989), the six domains of the flower-shaped germ have been formed. Each "petal" defines a new domain (sort of a peninsula with a large interface-to-volume ratio). In the core of each of these domains, the *L6* axis is rotated with respect to the initial *L6* axis and behaves like a new double-twist axis *L′6*. The limitation of the lateral extension of the branches creates the empty axial core of the germ. In this way, a regular twist between columns leads to the division of the germ into six branches that will themselves further divide into six parts, and so on. This evolution is sketched on Fig. 12. The left-handedness of the branches reveals that the twist between columns is right handed. In fact, in our system, dendritic growth and twist effects are not perfectly coupled. An excess of twist is accumulated before the dendritic growth allows the new series of double-twist axes to form. This excess of twist is relaxed along twist walls parallel to the direction of the columns (easily visible in Fig. 5 *a*, for example).

Although the division of the germs into six branches is a constant feature, the global shape of the germs may vary and form either a cylinder (Fig. 7) or a "diabolo" (Figs. 4 and 5). The former are rare and very small, whereas the latter are frequent and may be large. We suspect the bending properties of the columns to be responsible for this macroscopic shape of the germs. A certain flexibility of the columns allows the branches to coil around each other into helical paths and to form a cylindrical germ (Fig. 13 *a*). On the contrary, rigid columns will avoid this curvature of the branches. The branches would thus diverge into a diabolo shape (Fig. 13 *b*). Taking into account the relative amounts of the two kinds of germs, the rigidity of the columns would be the rule in these high-salt conditions, and their flexibility would be a particular case. From the observation of another type of germ (helical tubules) in low-salt conditions (Leforestier and Livolant, manuscript in preparation), we may suspect cylindrical germs to form in regions of slightly different ionic concentration, but we did not control their formation.

Last, splay configurations have been detected by electron microscopy analysis of the germs. To account for this splay,

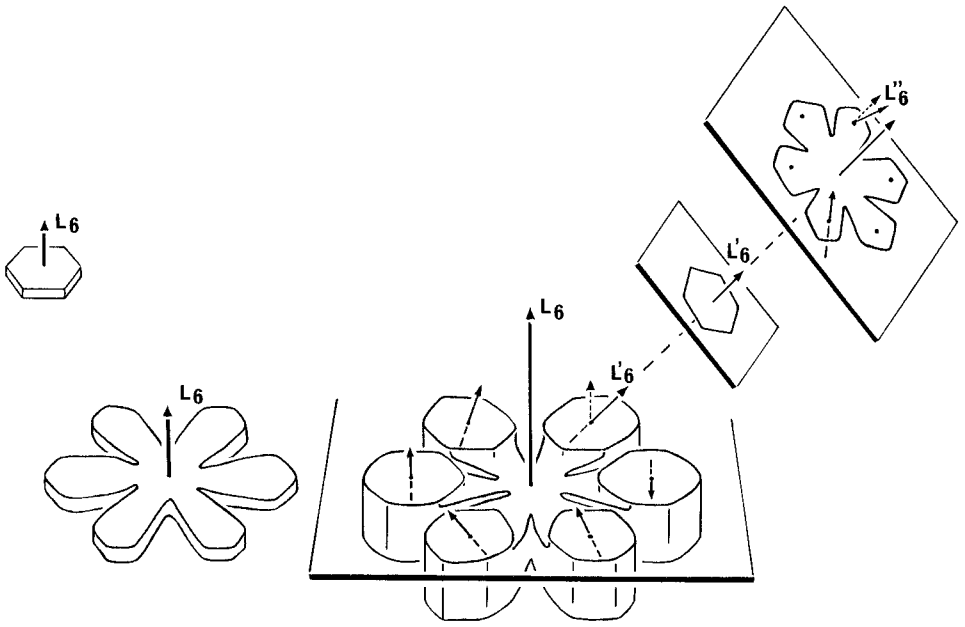

FIGURE 12 Competition between double-twist configurations and hexagonal packing leads to the individualization of the six branches. In small germs, the double-twist effect is small, and all molecules align nearly parallel to the *L6* axis. When the germ enlarges, the hexagonal packing creates dendritic shapes and defines six domains. In each of them a new hexagonal axis can be defined (*L′6*), oblique to *L6*, which becomes a new center of double-twist configuration. This domain itself will later subdivide into six other domains with new *L″6* double-twist axes, and so on.

columns must be added to the structure to keep a constant density. As thoroughly analyzed by Bouligand (1980a,b), defects may be edge or hybrid disclinations (both edge and a screw), with the defect line (L) normal to the direction of the columns (n). For small values of the Burger vector (b), three defect lines follow these conditions: the hybrid dislocation defined by b oblique to L, $L \perp n$, $b \perp n$, with $b = a$ (Fig. 14 *a*) and dislocations defined by $b \perp L$, $L \perp n$, and $b \perp n$, where the Burger vector (b) equals a and $a - a'$ (Fig. 14, *b* and *c*). These three defects were called, respectively, H1, E3, and E4 in a previous analysis of DNA columnar phases (Livolant, 1991). These three defect lines introduce splay

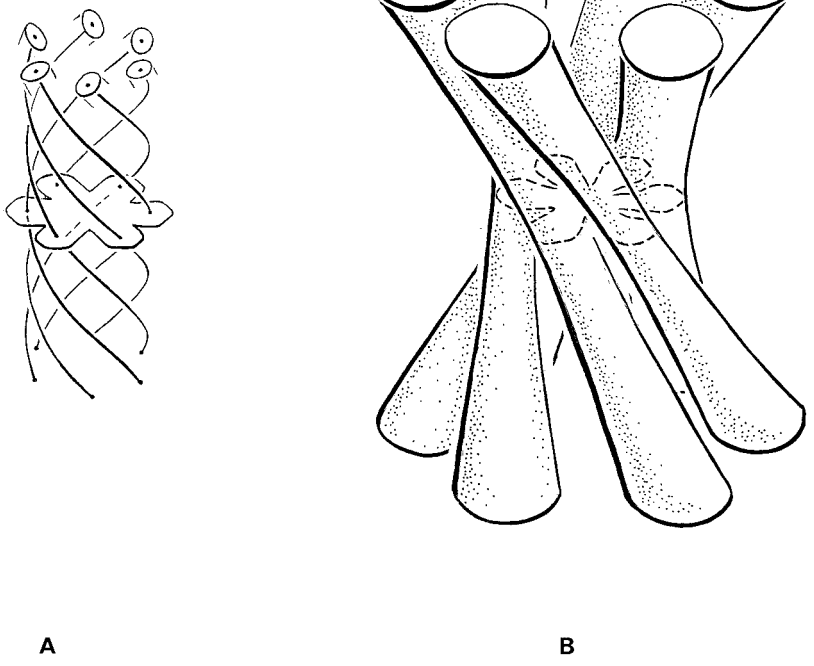

FIGURE 13 Global shapes of the germs, either cylindrical (*a*) or "diabolo" (*b*). In both cases, right-handed twist leads to left-handed helical germs. In *a*, branches follow true helices and the germ is cylindrical. In *b*, the six branches diverge.

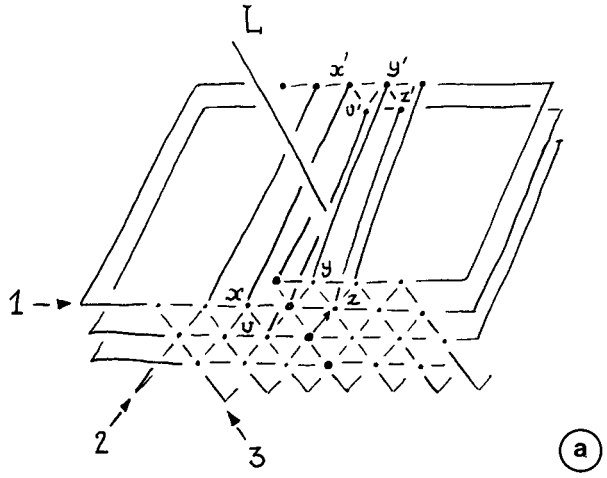

DISLOCATION H1

b oblique L L⊥n b⊥n b=a	Number of added columns	Number of added layers
Along planes 1	1	screw
Along planes 2	1	0
Along planes 3	0	1

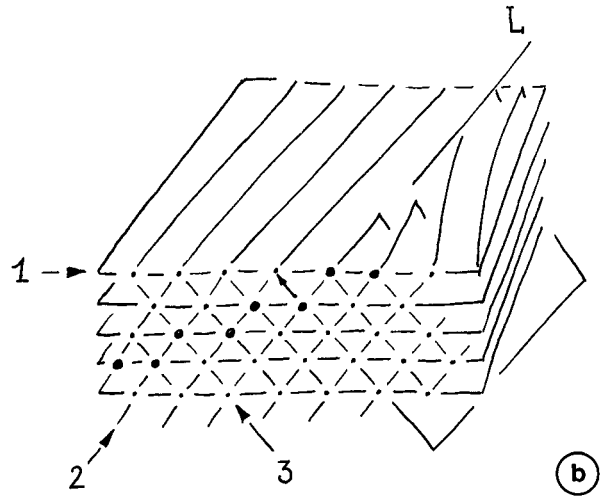

DISLOCATION E3

b⊥L L⊥n b⊥n b=a	Number of added columns	Number of added layers
Along planes 1	2	0
Along planes 2	2	0
Along planes 3	1	0

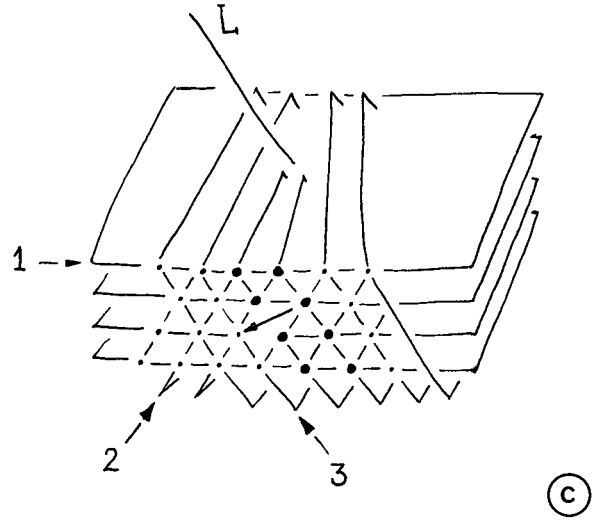

DISLOCATION E4

b⊥L L⊥n b⊥n b=a-a'	Number of added columns	Number of added layers
Along planes 1	2	0
Along planes 2	2	0
Along planes 3	0	2

FIGURE 14 Structure of the main defects, which may account for the introduction of new columns in the structure (splay). The number of added columns and added layers is indicated for the three directions of the hexagonal network. (*a*) Hybrid H1 dislocation (edge and screw) with $L \perp n$, b oblique L, $b \perp n$, and $b = a$. (*b*) Edge E3 dislocation with $L \perp n$, $b \perp L$, $b \perp n$, and $b = a$. (*c*) Edge dislocation with $L \perp n$, $b \perp L$, $b \perp n$, and $b = a - a'$.

between columns in the layers and splay between layers. We may notice that the number of added columns or added layers depends on the defect line but also on the reticular planes under consideration. Therefore, the splay introduced by a given defect line is not the same in all directions of the lattice. Taking into account the diameter of the columns (~11.5 nm), the presence of these defects should be detected, but surprisingly they were not. We suspect the insertion of additional layers to produce complex staircase patterns and formation of lacunae, disturbing the layered structure and preventing the clear observation of the defect structure. Splay is probably absent from the small cylindrical germs, but it could occur in the large ones because of the rigidity of the columns.

Such a complex growth process may lead to a variety of 3D geometries by varying the twist angle between columns, the twist angle between successive double-twist axes, the facetting parameters, and the rigidity of the columns. Energies involved should also be estimated to further understanding. From this study, it appears that both rotation of the hexagonal lattice (in the double-twist configurations) and rotation of the nematic director (along twist walls) occur in these germs. We may also wonder whether gaps between branches could be assimilated to twist walls filled with the isotrophic solution. In that sense, such 3D chiral germs may be considered to be a kind of moiré phase theoretically predicted by Kamien and Nelson (1995) but not yet observed experimentally.

Relevance to the chiral structure of eukaryotic metaphase chromosomes

In our liquid crystalline columnar phases the concentration of NCPs (310–485 mg/ml) is close to the concentration determined for eukaryotic chromosomes (433 ± 74 mg/ml) (Bohrmann et al., 1993). Despite the important differences between in vitro and in vivo systems (mainly the absence of linker DNA between NCPs and additional proteins such as H1 histones), we assume the interactions responsible for the liquid crystalline order to also be involved in the organization of chromatin and chromosomes. In this hypothesis, the chirality revealed in our model systems should also appear in chromosomes. The helical structure of chromosomes was reported in meiotic chromosomes of plant cells and observed later on in many other mitotic chromosomes through prophase to metaphase. It was especially enhanced by the use of hypotonic solutions of special salt composition, which was suspected to induce the release of some chromosomal components (Ohnuki, 1968). More recently, Boy de la Tour and Laemmli (1988), using gentle preparation methods, studied the three-dimensional folding of the scaffold in partially histone H1-depleted chromosomes. They confirmed that a few chromosomes keep a regular helical scaffold, while most of them are fully extended, and hypothesized a possible structural transition between the coil and extended conformations. The helical structure of eukaryotic chromosomes was also observed without any chemical treatment, by micromanipulation and micropipette aspiration: after extensive elongation, chromosomes relax into helical strands, and both left- and right-handed curls are observed (Houchmandzadeh et al., 1997).

Without considering any chromosomal model in particular, we suspect the helicity of the eukaryotic chromosome to originate from the competition between intrinsic columnar and chiral ordering, as in our system. The above-mentioned chemical or mechanical treatments would relax constraints imposed on the chromatin organization, thus leading chromosomes to adopt a helical conformation. Twisting the two extremities of a bundle of threads in opposite directions can easily cause this. In this way, twist is introduced between the threads. The bundle remains straight as long as a tension is applied at the extremities of the bundle, but removing this tension causes the thread to relax into a helix, thus reducing the local twist between the threads. The number of coils depends on the amount of twist introduced, and the handedness of the helix is opposite the handedness of the twist that has been introduced (right-handed twist leads to a left-handed helix, and conversely). In chemically treated chromosomes, the number of gyres was shown to be related to the length of the chromosome, as would be expected in this hypothesis. But in chromosomes the direction of coils was described as randomly either right-handed or left-handed and of opposite handedness in sister chromatids (Ohnuki, 1968; Boy de la Tour and Laemmli, 1988). This may seem surprising, but the twist handedness is not strictly determined by the handedness of individual molecules (Harris et al., 1999). The macroscopic pitch depends on both molecular chiral parameters and molecular orientational correlations. Because these correlations may vary with temperature, pH, pressure, etc., twist inversions may occur in this way. Taking into account the complexity of native chromatin and its local ionic environment, local left-handed or right-handed twist may be possible, leading to right- or left-handed coils, respectively. A more detailed analysis of the macroscopic and microscopic structural details of native chromatin should help to further the understanding of these structures.

We thank Yves Bouligand for his critical reading of the manuscript.

This work was supported by grants from the Association pour La Recherche sur le Cancer (ARC 6473).

REFERENCES

Bohrmann, B., M. Haider, and E. Kellenberger. 1993. Concentration evaluation of chromatin in unstained resin-embedded regions by means of low dose ratio-contrast imaging in STEM. *Ultramicroscopy.* 49: 235–251.

Bouligand, Y. 1980a. Defects and textures of hexagonal discotics. *J. Physique.* 41:1307–1315.

Bouligand, Y. 1980b. Geometry of (non smectic) hexagonal mesophases. *J. Physique.* 41:1297–1306.

Boy de la Tour, E., and U. K. Laemmli. 1988. The metaphase scaffold is helically folded: sister chromatids have predominantly opposite helical handedness. *Cell.* 23:937–944.

Harris, A. B., R. D. Kamien, and T. C. Lubensky. 1999. Molecular chirality and chiral parameters. *Rev. Mod. Phys.* 71:1745–1757.

Houchmandzadeh, B., J. F. Marko, D. Chatenay, and A. Libchaber. 1997. Elasticity and structure of eukaryote chromosomes studied by micromanipulation and micropipette aspiration. *Biophys. J.* 139:1–12.

Kamien, R. D., and D. R. Nelson. 1995. Iterated moiré maps and braiding of chiral polymer crystals. *Phys. Rev. Lett.* 74:2499–2502.

Kamien, R. D., and D. R. Nelson. 1996. Defects in chiral columnar phases: tilt-grain boundaries and iterated moiré maps. *Phys. Rev. E.* 53: 650–666.

Kléman, M. 203. 1985. The coexistence of cholesteric and 2-dimensional orders. *J. Physique.* 46:1193–1191.

Leforestier, A., and F. Livolant. 1994. DNA liquid crystalline blue phases. Electron microscopy evidence and biological implications. *Liquid Crystals.* 17:651–658.

Leforestier, A., and F. Livolant. 1997. Liquid crystalline ordering of nucleosome core particles under macromolecular crowding conditions: evidence for a discotic columnar phase. *Biophys. J.* 73:1771–1776.

Livolant, F. 1984. La structure cristalline liquide de l'ADN in vivo et in vitro. Thèse d'Etat Paris.

Livolant, F. 1991. Supramolecular organization of double stranded DNA molecules in the columnar hexagonal liquid crystalline phase. *J. Mol. Biol.* 218:165–181.

Luger, K., A. W. Mäder, R. K. Richmond, D. F. Sargent, and T. J. Richmond. 1997. Crystal structure of the nucleosome core particle at 2.8 Å resolution. *Nature.* 389:251–260.

Ohnuki, Y. 1968. Structure of chromosomes. I. Morphological studies of the spiral structure of human somatic chromosomes. *Chromosoma.* 25:402–428.

Robinson, C., J. C. Ward, J. C., and R. B. Beevers. 1958. Liquid crystalline structure in polypeptide solutions. *Disc. Faraday Soc.* 25:29–42.

Samulski, E. T., and A. V. Tobolski. 1974. *In* Liquid Crystals and Plastic Crystals, Vol. 1. Gray and Winsor, editors. Wiley, New York. 174.

Wright, D. C., and N. D. Mermin. 1989. Crystalline liquids: the blue phases. *Rev. Mod. Phys.* 61:385–431.

Yan, Gu, and T. C. Lubensky. 1997. Chiral discotic columnar phases in liquid crystals. *J. Physique II.* 7:1023–1034.